

METROLOGY METHODS FOR ISOLATING PROFILE FORM, WAVINESS, STEPS, AND TWIST FROM SCANS OF SMALL-SCALE LAMINAR FLOW WIND TUNNEL MODELS

Christoph Hiemcke[1], Ryan Buth[2], Christopher Schneider[2] & Christopher J. Jones[1]

[1]General Atomics Aeronautical Systems, Aerodynamics, San Diego, USA
[2]General Atomics Aeronautical Systems, Metrology, San Diego, USA

Abstract

The purpose of this paper is to find a way to communicate surface tolerances to wind tunnel model makers and metrology teams. Traditionally, the model buyer only specifies a uniform surface tolerance and a maximum roughness. Our method adds surface tolerances at the level of individual airfoils, i.e., at multiple spanwise sections extracted from the point cloud. Each airfoil is divided into chordwise segments, each with its own surface tolerance so as to avoid surface waves that lead to premature transition by amplifying Tollmien-Schlichting (T-S) waves.

At each spanwise cut we perform best fits for a partial circular arc near the leading edge (LE), and an isosceles trapezoid near the trailing edge (TE), with the purpose of identifying the positions of the LE and TE, as well as the LE radius, the LE camber angle, the TE camber angle, the TE thickness, and the TE closure angle. Connecting the LE and TE yields the chord line which provides us with the chord length and the pitch angle (local angle of twist). We are thus able to align the ideal “as-designed” airfoil and the scanned “as-built” airfoil: we align the LEs, then rotate the cloud so that the chordlines are coincident, and finally uniformly scale the point cloud in order to achieve the same chordlengths. We can also use the LE and TE to split the point cloud into a top and a bottom half.

Once we have done this at all spanwise sections, we have the twist distribution. We can then split each chord at 70%c, 75%c, 80%c, and 85%c, and then draw spanwise lines to connect all the LEs, TEs, and in-between chordwise stations. The straightest of these lines is closest to the axis of twist, and we can use it to determine the dihedral angle.

With the ideal and scanned airfoils aligned, we separate the form and the texture using the two-dimensional point cloud. That process begins by fitting a partial circular arc near the leading edge (LE), and an isosceles trapezoid near the trailing edge (TE), as we did before. We use the endpoints of the arc and of the forward edge of the trapezoid to split the top and bottom point clouds. At about five additional chordwise stations we further split the top and bottom point clouds. At each of the split locations we use all nearby points (within about 0.5%c of the split) to fit a cubic polynomial from which we harvest the slope at that split location. Armed with the location and slope at each split location on the top, we fit a series of quintic polynomials to arrive at the upper form of the scanned profile. Marching along the surface of the upper scanned form we use the local normal to compute the distance to the nearest point in the point cloud, thus providing us with the upper texture (the sum of the roughness and all imperfections). We do the same on the lower side.

Next we plot the upper texture and its point-to-point slope, especially in order to define locations with sudden slope changes that indicate the presence of steps or flat spots. We further split the point cloud at those locations and perform a new set of cubic and quintic fits in order to more clearly

identify flat spots.

Finally we perform fast Fourier transforms (FFTs) and wavelet transformations to identify the wavelengths, amplitudes, and locations of waves. We compare the wave properties to the surface tolerances to determine whether they will lead to transition.

We illustrate our process by applying it to a wind tunnel model of the PRANDTL-D flying wing with a span of two feet and a representative chord of two inches. Resolving the relevant defects, wavelengths and amplitudes requires the scanner to have a horizontal resolution of 11 microns, and a vertical resolution of 4 microns.

Keywords: Metrology, wind tunnel model, transition

1. Motivation, Introduction and Background

The author has struggled for many years to find a way to meaningfully specify manufacturing tolerances (including surface tolerances) for small-scale wind tunnel models, and to verify them following construction. He was reasonably successful in verifying overall rigging and surface finishes. Some model makers used coordinate measurement machines (CMM) with contact probes to collect hundreds of points (Figure 1) and that method is reasonably successful in verifying the overall profile shapes and twist distribution.

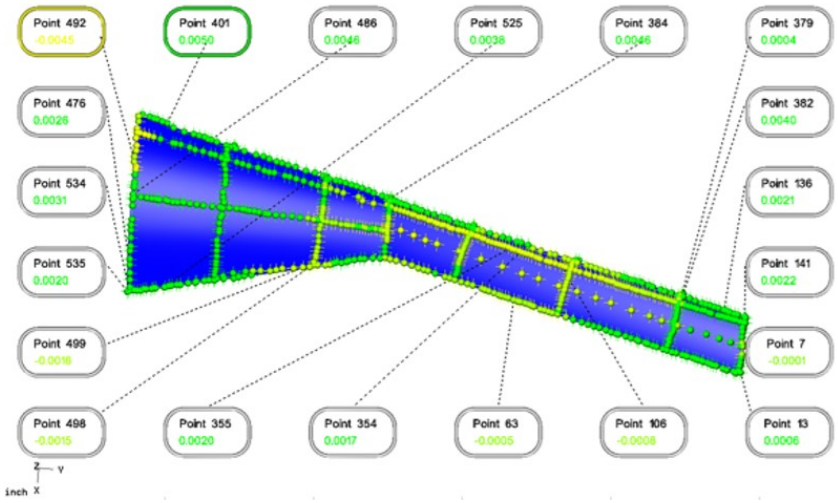


Figure 1 – Grid of CMM points on a wing.

But the method fails to resolve the LE and TE regions. As Figure 2 shows, we really cannot conclude much about the quality of the LE or TE shape if we only use a few dozen sample points. Note that the tolerance band in Figure 2 (especially near the LE and TE) suggests that either significantly more samples were taken, or a curve was fit through all or some of the 32 sampling points.

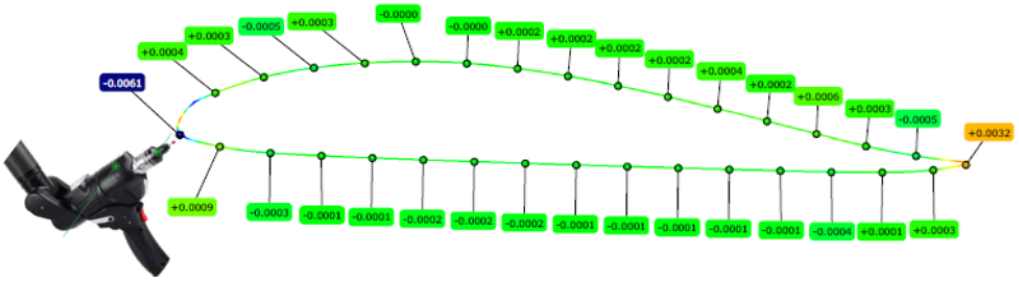


Figure 2 – Grid of CMM sampling points on an airfoil, with tolerance band.

The tolerance band is colored by the normal deviation between the point cloud (or the curve fit through the point cloud) and the ideal airfoil. Based on the value at the TE the tolerance was probably 4 thou (102 microns). The example in Figure 3 shows how geometric dimensioning and tolerancing (GD&T) is used to specify a tolerance.



Figure 3 – Using GD&T to create a tolerance band, from [1].

Past efforts related to the desire to scan the geometries of wind tunnel models, model aircraft, and full-scale airplanes are dominated by efforts to scan the blades of turbomachines, such as the fan blades of turbofan aircraft engines [2-6]. Fan blades, compressor blades, and turbine blades are scanned following manufacture for quality control (QC) purposes. They are also often scanned during overhauls to detect and quantify any damage, and to determine whether a given blade can be reused or repaired. Also, the stacking sequence of the different spanwise cuts is analyzed to make sure that the blade remains mass balanced, and the inspectors are probably also making sure that the twist distribution is within tolerance. Related to the scanning of turbomachinery blades is that of propellers [7], wind turbine blades, and helicopter blades.

1.1 Common CAD Procedure, CAD errors, and Scanning Procedure

Let us consider the case where a standard method was used in a CAD system to generate the wing. That method usually starts with a fairly coarse set of airfoil coordinates, and the CAD operator must usually fit one or more curves through those points. The underlying set of coordinates is usually too coarse in the LE region, resulting in the incorrect LE radius and an incorrect location of the LE point. One may also end up with unintended flat spots (see Figure 4).

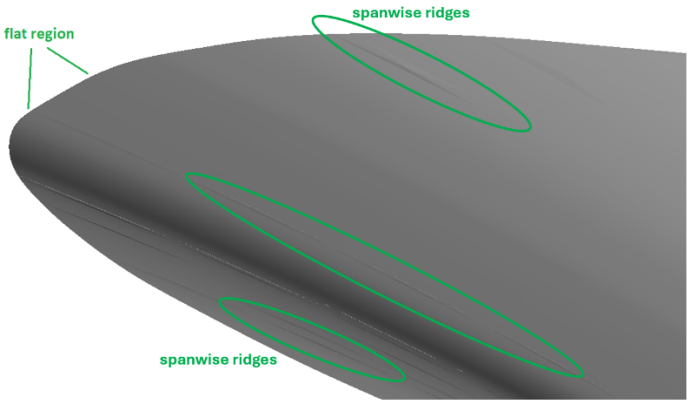


Figure 4 – Typical CAD geometry problems on a wing.

For a given set of airfoil coordinates, there are different ways to perform the curve fit(s) through the points, each one resulting in a different shape. For example, one might accept the LE point and TE point (top left of Figure 5) and create separate curve fits for the top and the bottom. One might force the curve fit to be normal to the x-axis at the LE point. Alternatively, one might force the slopes of the top and bottom to be the same at the LE point, but one might not force it to be perfectly vertical. The two approaches will result in different shapes.

Once two or more profiles are defined and curve fitted, the CAD operator can add sweep, dihedral, and twist. Here it is important to know where the twist axis is located: a twist axis at the hinge line will produce a different geometry than a twist axis at the TE.

A further CAD complication is that we may use different airfoil families at the root, tip, and intermediate spanwise station. This gives rise to differences in airfoil topology. A good example is when there is a significant difference in LE radii. When lofting between the airfoils that are

topologically different, the resulting surfaces often have creases, folds and/or ridges along the sweep direction, and one may also see concave panels.

Yet another CAD complication occurs when surfaces or volumes undergo Boolean operations such as splitting. The process sometimes results in unintended surface waves and wrinkles. If the CAD model is exported in a standard format, such as STEP, and if the export tolerances are not tight enough, there may be further unintended shape changes.

The finished CAD object (the ideal wing) is sent to manufacturing to be built, resulting in the "as-built" wing.

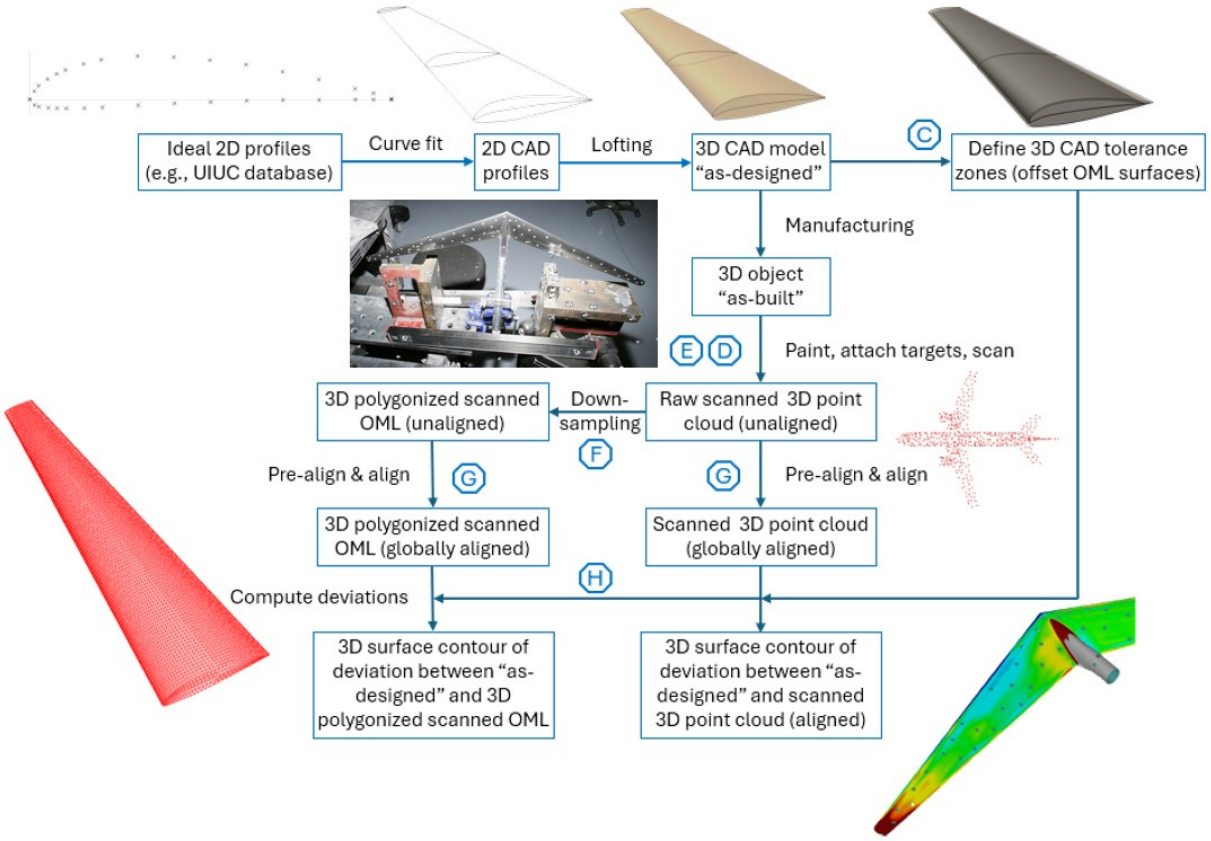


Figure 5 – Common CAD and scanning procedure.

As shown by Step C in Figure 5, one way to define the tolerance zone is to offset the wing surface, or outer mold line (OML), in both directions to create two surfaces separated by the tolerance value.

Once the model is built, it is mounted and prepared for scanning, which often involves a coat of matte paint and the attachment of targets. If the model is small, a single scanner may be sufficient, and perhaps also a single pass. Sometimes multiple scanner types have to be used. If the resolution of the scanner is not high enough, multiple passes are made in order to increase the point cloud density. Steps E and D in Figure 5 result in the raw, unaligned 3D point cloud. One option is to work directly with that point cloud, the other is to polygonize the point cloud, which typically involves automatic down-sampling (Step F in Figure 5). The user may not have much control over the down-sampling, and it may in fact destroy some of the features we are looking for. An additional step is to fit surfaces such as splines to the polygonized point cloud, resulting in a reverse-engineered model. The fitting of surfaces often gives rise to further unintended distortions of the geometry: for example, a spline near the LE may undershoot the actual geometry, as shown in Figure 6. Similarly, a spline that includes the TE is likely to round any sharp edges there.

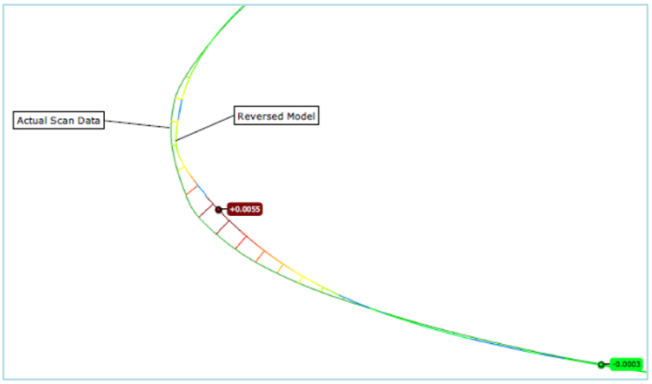


Figure 6 – Poor fit of a spline at the LE.

To do the pre-alignment, the operator typically imports the ideal "as-designed" CAD geometry with its global coordinate system into the session showing the raw point cloud. During the pre-alignment step, the operator might roughly align the noses from the point cloud and from the CAD model. Similarly, they might roughly align the same wingtips from the two models. After that, the final alignment is often a least-squares minimization of the normal distances between the CAD and the point cloud. Note that this alignment method (Step G in Figure 5) does not take into account any of the topology details of the airplane. For example, the longitudinal axis of the point cloud or its polygonized cousin might be yawed and pitched with respect to the longitudinal axis from the CAD model. Similarly, the overall least-squares fit may produce a wing whose dihedral and twist distribution differs significantly from the CAD model.

Once the alignment is accomplished we compute the normal deviations (Step H) and we check whether the point cloud is within the tolerance zone everywhere. On the bottom right of Figure 5 we show the PRANDTL-D wind tunnel model with contours of normal deviation. The contour suggest that the left wing of the model may have more outboard dihedral than the CAD model, or perhaps the outboard airfoil thickness is too high – there really is a need to investigate further: we must perform spanwise cuts of the 3D point cloud to extract a 2D point cloud at each section, and to derive an "as-built" airfoil from each.

1.2 Scanning SDSU's 2-Foot PRANDTL-D

The methods described above were applied by the second and third authors during the scan of the San Diego State University (SDSU) 2-foot wind tunnel model of the PRANDTL-D [8]. To avoid reflections, the model was spray-painted with Magnaflux SKD-S2 Spotcheck Developer. The model was mounted and DIA 1.5mm optical targets were attached. The overall coordinate system was created using a Tritop Photogrammetry system. An ATOS Core 80mm scanner was used to perform the actual scan, with careful attention to the LE and TE regions. The resulting point cloud had an average chordwise resolution of 1.8 thou (46 microns), with about 2200 points per spanwise cut.

We found that alignment of the model was not trivial, with the root incidence of the aligned point cloud being about one degree off the expected value. During the design of a wind tunnel model, it is important to include a leveling plate that usually attaches to a box-shaped bay near the moment reference center (MRC) whose bottom face is perfectly parallel to the aircraft's longitudinal axis, and whose side walls are perfectly parallel to the aircraft's symmetry plane. The leveling plate is used to align the model in the wind tunnel. In addition, the floor and walls of the bay are very useful for aligning the point cloud.

We used the "Geomagic Design X" software to fit a patchwork of NURBS surfaces to the point cloud in order to create a first reverse-engineered model. Our second reverse-engineered model utilized an orthogonal grid of parametric surfaces. The red line in Figure 7 shows a polyline resulting from the heavily down-sampled point cloud (just 280 chordwise points), while the blue line is the resulting curve fit, illustrating how the finite trailing edge with its sharp edges is incorrectly represented by a smooth curve.

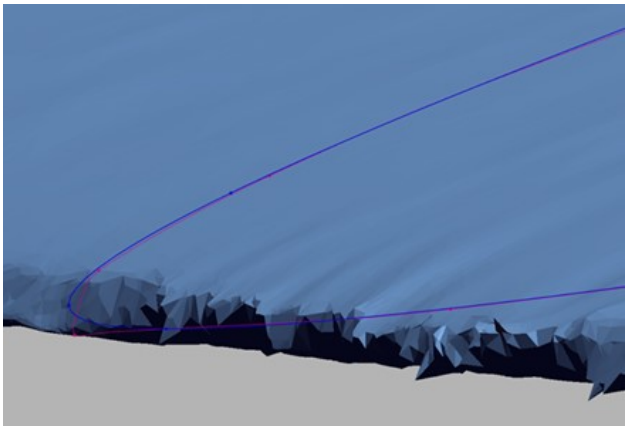


Figure 7 – Poor fit of a spline at the TE.

2. Surface Tolerances Based on Trip Heights

We have traditionally specified the surface tolerance to be smaller than the local height of a strip that would trip the flow into turbulence. When pressed for time, we use the Braslow-Knox (B-K) flat-plate criterion, but we prefer to use the Van Driest and Blumer (D-B) method [9] since it utilizes boundary layer heights specific to the airfoil and its flight condition. We use XFoil to determine the boundary layer height, which is then used in the D-B method to compute the height (e_{crit2}) of trip dots and steps that will transition the flow. We do this at multiple chordwise stations, and at multiple flight conditions (such as multiple angles of attack).

The example in Figure 8 shows results for the mid-span profile of the PRANDTL-D, with a 2" chord and at Re = 0.2M, analyzed at pitch angles of -1°, 3°, and 9°. We see that steps near the LE need to be smaller than 3 thou or about 90 microns (see the table in Figure 12 below). Aft of the quarter-chord the critical height is about 5 thou.

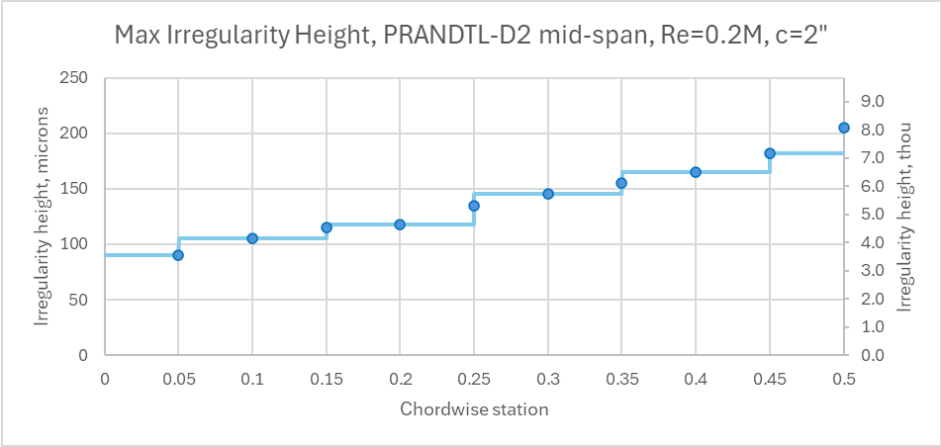


Figure 8 – Critical trip height for PRANDTL-D mid-span airfoil at Re=0.2 million.

3. Surface Tolerances Based on the Carmichael Criteria

Carmichael and his coworkers [10, 11] arrived at criteria for imperfections as well as waves. These were based on flight tests at high Reynolds numbers, so they may have limited applicability in the case of small wind tunnel models at low speeds.

With regard to steps, rounded steps, gaps, and ramps they installed a natural laminar flow (NLF) glove on a Beech T-34C (low-wing, tractor propeller).

With regard to waves they flight tested the X-21, which was a high-wing jet with two jet engines by the tail. Application of the Carmichael criterion for waves to the case of the PRANDTL-D wind tunnel model yields (assuming units of inches):

$$\frac{h}{\lambda} = \sqrt{\frac{59{,}000 \cdot c \cdot cos^2(\Lambda_{LE})}{\lambda (Re_c)^{1.5}}} = \sqrt{\frac{59{,}000 \cdot 2 \cdot cos^2(24°)}{\lambda (200{,}000)^{1.5}}} \quad (1)$$

$$h = 0.015407\sqrt{\lambda} \quad \text{(inches)} \quad (2)$$

Initial recommendations were to divide this value by 3 if there were multiple wave peaks, but that value has moved to close to 1 with growing experience. This suggests that a single wave period is almost as effective as a wave train.

4. Surface Tolerances Based on Stability Theory, with Hartree Pressure Gradient

We now consider waves that destabilize the Tollmien-Schlichting waves in a flow with nonzero pressure gradient. We look at stability diagrams that are based on boundary layer stability theory in the form of the Orr-Sommerfeld equations. We again turn to XFoil to analyze the airfoil, in this case computing the distributions of the edge velocity, $U_e(s)$, boundary layer thickness, $\delta_1(s)$, and the shape parameter $H_{12}(s)$. We enter the plot in Figure 9 using H12 to determine the Hartree parameter, β_H, which is defined as [12]:

$$\beta_H = \frac{2s}{U_e}\frac{\partial U_e}{\partial s} \quad (3)$$

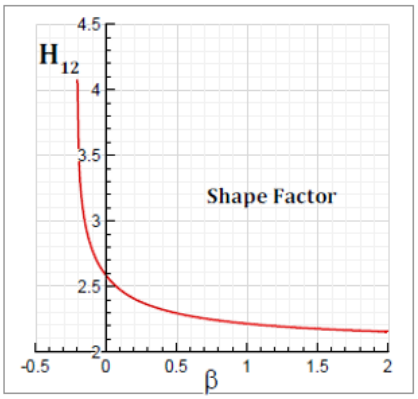


Figure 9 – Plot to find the Hartree parameter, from [12].

Note that the Reynolds number based on boundary layer height is defined as:

$$Re_{\delta 1} = \frac{\rho_\infty v_\infty \delta_1}{\mu_\infty} \quad (4)$$

We enter the stability diagram (Figure 10) using $Re_{\delta 1}$ and move upwards to find the two intercepts with the β-contour of interest. From there we trace to the left to determine the corresponding frequencies.

We translate the frequencies into wavelengths using the freestream velocity (180 ft/s in our case) to find that typical wavelengths range from 0.25 mm to 7.5 mm (9.8 to 295 thou). For comparison, with a zero pressure gradient the shortest wavelength is about 2 mm.

We use the Carmichael Criterion for waves (Equation 2) to find that wavelengths of 0.0098" to 0.295" correspond to amplitudes of 1.5 to 8.4 thou (38.7 to 213 microns). We will use these values later (see the table in Figure 12).

Resolving the wavelength (0.25 mm) into 16 points and the trough-to-peak amplitude (38.7 microns) into 8 points yields horizontal and vertical scanner resolutions of 15 and 4.9 microns, respectively (again refer to the table in Figure 12).

Referring again to the stability diagram in Figure 10 we note that over the forward 15% of the top surface, destabilizing wavelengths range from 0.25 to 0.7 mm. Over the forward 15% of the bottom surface the range is from 0.4 to 1.1 mm. We will see these numbers again later (see Figure 11).

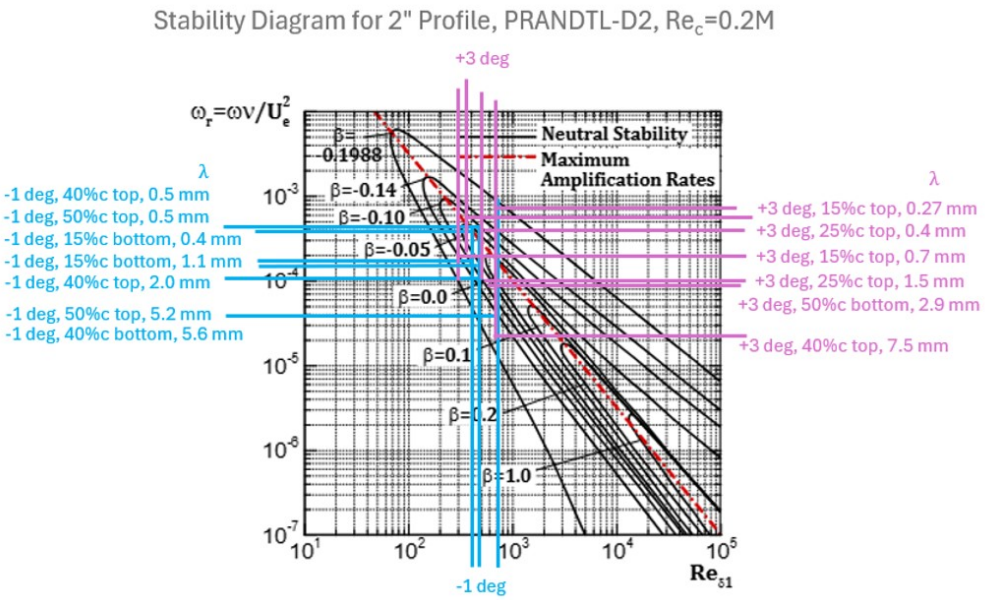


Figure 10 – Stability diagram.

5. Controlling Waves Using Surface Tolerances

A literature review revealed that the best way to control surface waves is to use an extended version of the surface texture symbol [13,14]. Up to this point, we had only used it to control the roughness so that it stays below 32 microinches (0.81 microns), since that is the typical finish for milled and turned aluminum. In Figure 11 below we propose a method for controlling waves over multiple chordwise segments.

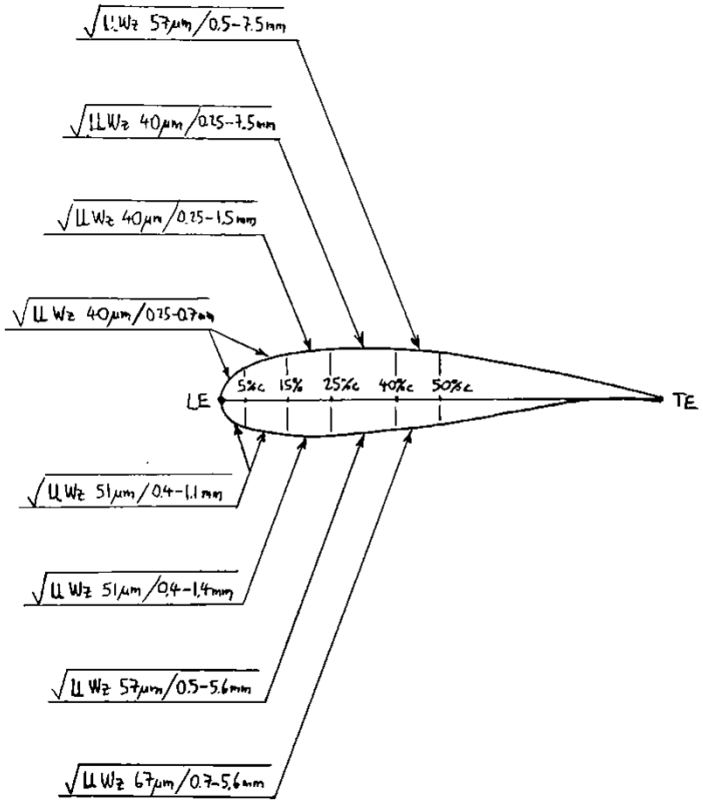


Figure 11 – Controlling waviness on the 2” PRANDTL-D2 airfoil via surface texture symbols.

For example, on the top surface over the forward 15%c we look for wavelengths between 0.25 and 0.7 mm, making sure that their amplitudes remain below 40 microns. This is based on the findings in the previous section.

6. Scanner Resolution Based on Critical Heights and Wavelengths

Figure 12 summarizes our findings up to now. In the bottom row of the table we recognize the horizontal and vertical dimensions of the waves over the forward 25% as slightly conservative versions of the 0.25 mm wavelength and the 40 micron height from the preceding section.

Feature/Mechanism, c=2", Re_c=0.2M	Feature dimensions (microns)						Scanner resolution (microns)					
	0-25%c		25-50%c		50-65%c		0-25%c		25-50%c		50-65%c	
	Horiz	Vert	Horiz	Vert	Horiz	Vert	Horiz	Vert	Horiz	Vert	Horiz	Vert
Steps, ridges	**90**	90	**150**	150			**11**	11	**19**	19		
Flat plate T-S, zero beta					**2000**	**110**					**125**	**14**
Flat plate T-S with Hartree Beta	200	**35**	400	**49**			12.5	**4.4**	25	**6.1**		

Figure 12 – Feature sizes and scanner resolutions for 2-ft PRANDTL-D2 model with 2" chord.

In the top row we recognize the critical height of 90 microns from the section on applying the D-B method to determine the critical height that will cause transition. It is the smallest of the vertical feature we must resolve. In case the feature is a S-curve instead of a ramp or step we need to resolve it using 8 intervals, so the horizontal resolution needs to be 11 microns.

The smallest vertical resolution is due to the wave height of 35 microns. Resolving that height into 8 intervals results in a vertical resolution of 4.4 microns.

We conclude that the scanner's horizontal and vertical resolutions need to be 11 and 4.4 microns, respectively.

7. Creation of a Fake 2D Point Cloud Based on PRANDTL-D Quarter-Span Airfoil

In Section 1.2 we discussed our scan of SDSU's 2-ft PRANDTL-D wind tunnel model, with its average chordwise resolution of 1.8 thou (46 microns). That resolution is significantly coarser than the required 11 micron resolution from the preceding section.

To develop and exercise our methodology we started with an ideal airfoil and systematically added defects to it. We started with the quarter-span airfoil from Marco's OpenVSP model [15] of the PRANDTL-D, which used the coordinates for the root and tip airfoils published by Al Bowers [16]. We used Microsoft Excel to insert a triangular wedge to create a finite TE of height 5 thou (127 microns). The chordlength of this "as-designed" airfoil is 2.133".

The first author used ChatGPT (GPT-5) and Claude 4.5 Sonnet to evolve a Python code (Python 3.11) that first increased the resolution of the airfoil to about 10,000 coordinate pairs and then added a normal step up, a normal step down, a flat spot, and a section with waves. It then added noise in the normal direction, and finally rotated the airfoil 8.5° nose-up. The first version of this fake 2D point cloud had exaggerated feature heights and is shown in yellow in Figure 13.

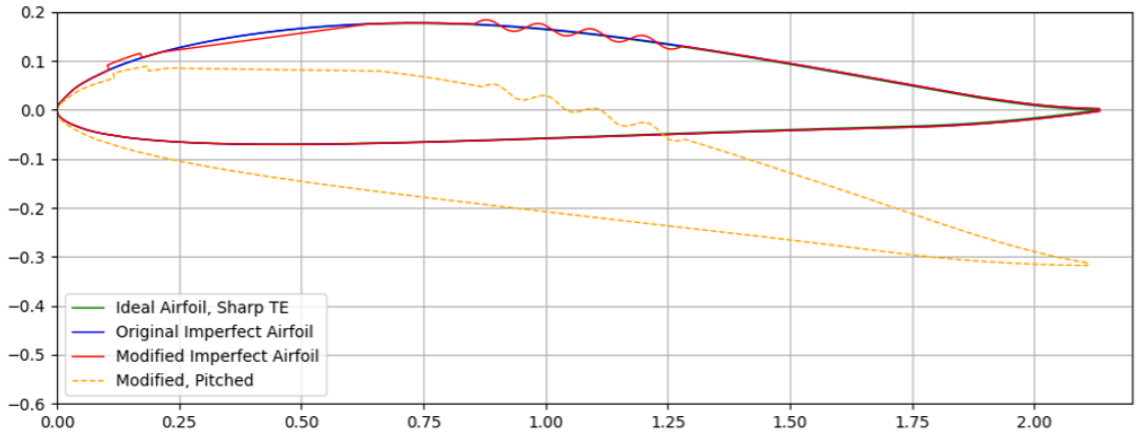


Figure 13 – Pitched, Imperfect airfoil with steps, flat spot, waves, finite TE, and artificial roughness.

8. Aligning the 2D Point Cloud by Finding the LE and TE

In Section 1.1 we discussed the traditional method of aligning the overall point cloud with the overall CAD model. Now we want to go beyond that, by creating spanwise cuts to extract 2D point clouds that represent the local airfoils. Each spanwise cut brings its own ambiguities because the points from the point cloud will rarely lie on the cutting plane, so some type of interpolation and/or nearest neighbor search is involved.

Once we have the 2D point cloud we need to estimate the locations of the LE and TE. Once we have the approximate locations, we can find the precise locations of the LE and TE.

Automatically estimating the locations of the LE and TE is not trivial, especially if the point cloud includes outliers. One method we tried was to first compute the centroid of all the points, and to define a large ellipse at that centroid. Using an optimizer, the major and minor axis of the ellipse were shrunk and the inclination varied until the ellipse touched three points (red line in Figure 14). Using the same centroid we defined a very small ellipse and allowed it to grow and pitch until it touched three points. We averaged the two ellipses to estimate the shape of the airfoil.

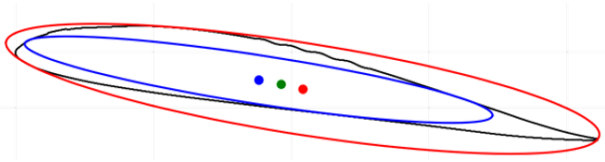


Figure 14 – Estimating LE and TE locations using ellipses.

A more robust way to automatically estimate the locations of the LE and TE may be to use methods from computer vision. Similar to the gamma correction for flatbed scanner images, one should be able to retain only those portions of the point cloud in which the points are densely clustered. One could then fit the best ellipse to the remainder, allowing one to estimate the LE and TE.

Once the LE and TE have been estimated, we can estimate the chordlength and we can define a LE region and a TE region. We can also define a preliminary x-z coordinate system.

Our next step is to define a partial circular arc near the LE. It has a 50-degree wedge angle, based on prior experience [17]. The optimizer varies its radius, inclination, and center location to best fit the point cloud over the forward 3%c (see Figure 15).

Similarly, we define an isosceles trapezoid near the TE. To perform the best fit we only use the two legs and the aft base. The optimizer varies the wedge angle (related to the TE closure angle), inclination angle (same as the TE camber angle), the aft base height (same as the TE height) and the center location to best fit the point cloud over the aft 3%c. The center of the aft base is the final TE location.

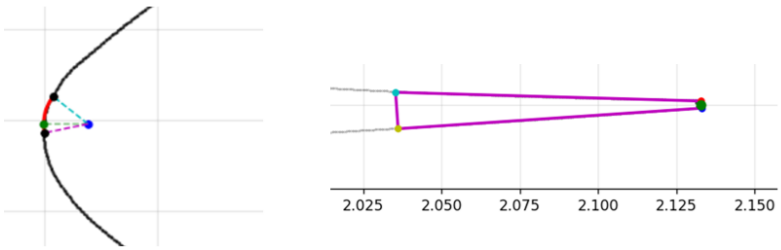


Figure 15 – Fitting a partial arc and an isosceles trapezoid.

We connect the LE and the TE to define the final chordline and the associated chordlength and pitch angle (Θ_y). By comparing this chordlength to the ideal one, we arrive at a scale factor, $h=h_x=h_z$. We can also use the LE and the TE to split the point cloud into a top half and a bottom half.

We begin the alignment by translating the LE point of the 2D point cloud to the LE point of the "as-designed" airfoil, through distance (t_x,t_z). The we rotate the point cloud through pitch angle Θ_y so that the two chordlines are coincident. Finally we scale the point cloud in both directions using the scale factor, h, so that the two TE points will also be coincident.

At this point we can march along the surface of the ideal airfoil to compute the local normal and to find the local normal distance (deviation) to the point cloud. We compare the deviation to the surface tolerance zone. With the airfoils properly aligned, this gives us a better sense for how close

our model is to the intended shape. Figure 16 shows a tolerance band whose thickness and color varies with the magnitude and sign of the deviation, and we can easily spot steps and waves.

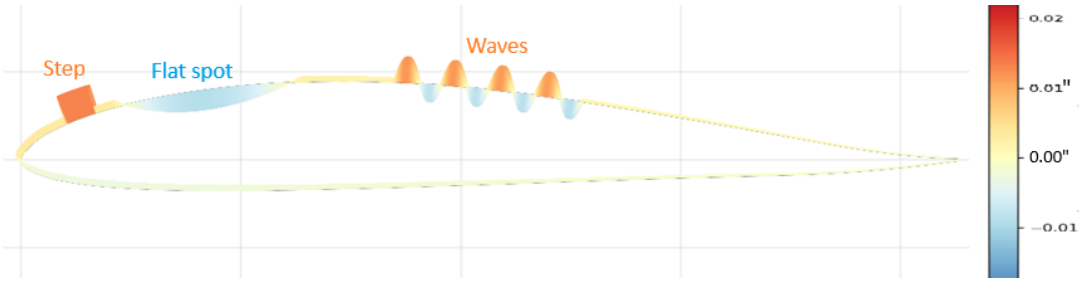


Figure 16 – Tolerance band on an airfoil.

Once we perform this procedure for every spanwise station of interest we will have the "as-built" twist distribution, and we can compare it to the intended one.

Next we will look for the axis of twist. We connect all the LE points with straight line segments. Similarly, we connect all TE points. Furthermore, we place points on the chordline of each airfoil at the 70%c, 75%c, 80%c, and 85%c stations. We use straight-line segments to connect all the points at the 70%c station. Do the same at 75%c, 80%c, and 85%c. Now look at the resulting six lines in the front view and the side view, and pick the one that is the straightest – we will use it as the axis of twist. In the front view, the axis of twist will also yield the dihedral angle. Figure 17 shows the spanwise sections ("Profilstrak") of the PRANDTL-D. It suggests that the axis of twist is close to the TE – it is probably at the control surface hinge line.

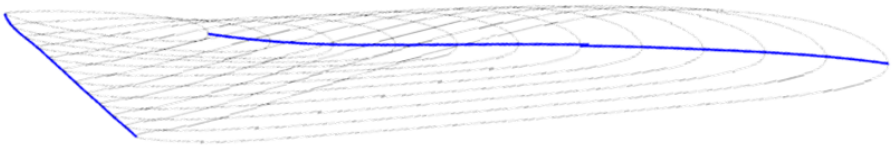


Figure 17 – Spanwise sections of the PRANDTL-D.

9. Splitting the 2D Point Cloud into Form and Texture via Quintic Polynomials

In the previous section we processed the 2D point cloud to determine the LE and TE positions. We did this by fitting a 50 circular arc at the LE and an isosceles trapezoid at the TE. In this section we will use the two endpoints of the arc and the two forward corners of the trapezoid as starting points for our curve fits.

Focusing first on the top half of the point cloud, and based on our prior experience with the PRANDTL-D airfoil [17], we create six segments by splitting it at 3%c, 7%c, 30%c, 60%c, and 80%c. At each of these chordwise stations, we select all points of the top point cloud that are within 0.5%c and fit a cubic polynomial through them (dashed blue lines in Figure 19), with the aim of computing the local slope at that chordwise station.

Next, and based on our prior work [17], we define a quintic polynomial for each segment. At each splitting point we force C0 and C1 continuity, making the location and slope the same on both sides of the point. Figure 18 shows the quintic polynomials fitted to the fake point cloud.



Figure 18 – Quintic polynomials fitted to the 2D point cloud.

We found that the curve fit is sensitive to the location of the splitting points, as well as the length of the cubic polynomials, especially if there is a nearby step or wave. For example, the close-up near the LE in Figure 19 shows how the presence of the step generates a bump in the curve produced by the quintic polynomials.

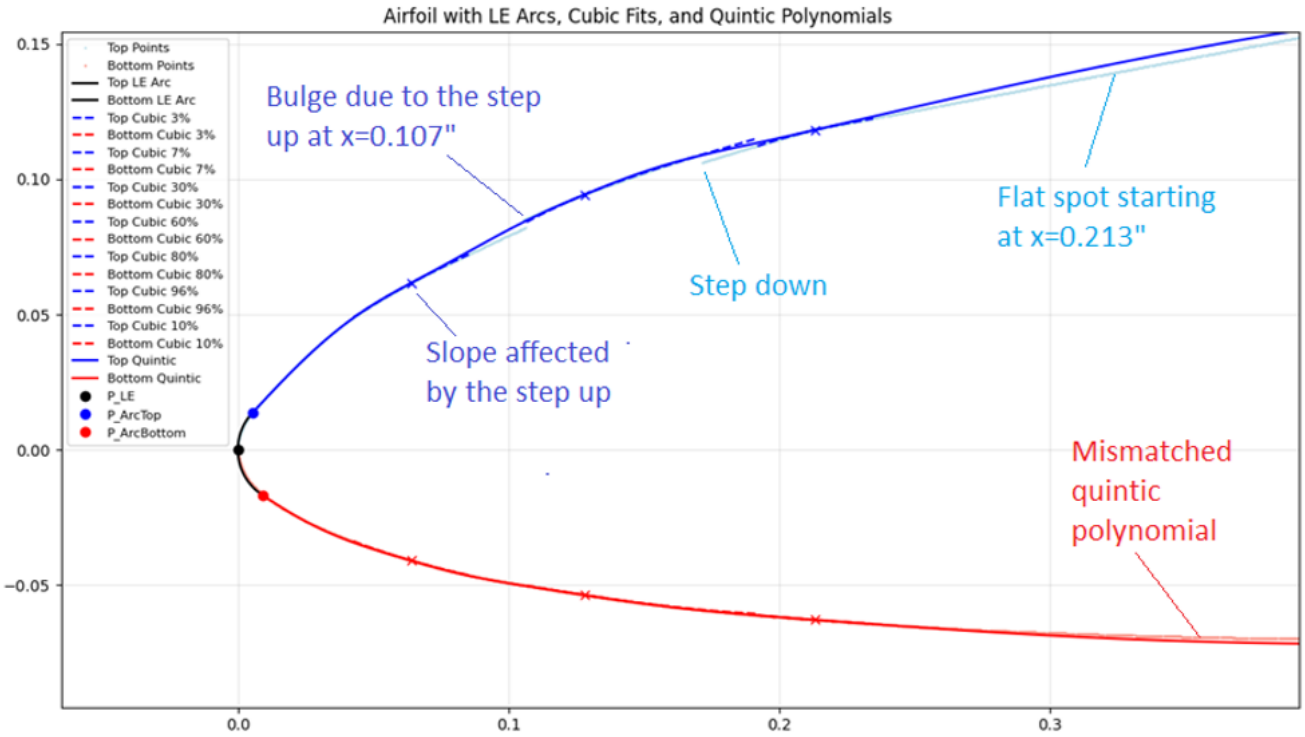


Figure 19 – Quintic polynomials near the LE.

In the region with the waves we find that the quintic polynomial fit is near the create of the waves on the upstream side, whereas it is centered on the downstream side (Figure 20).

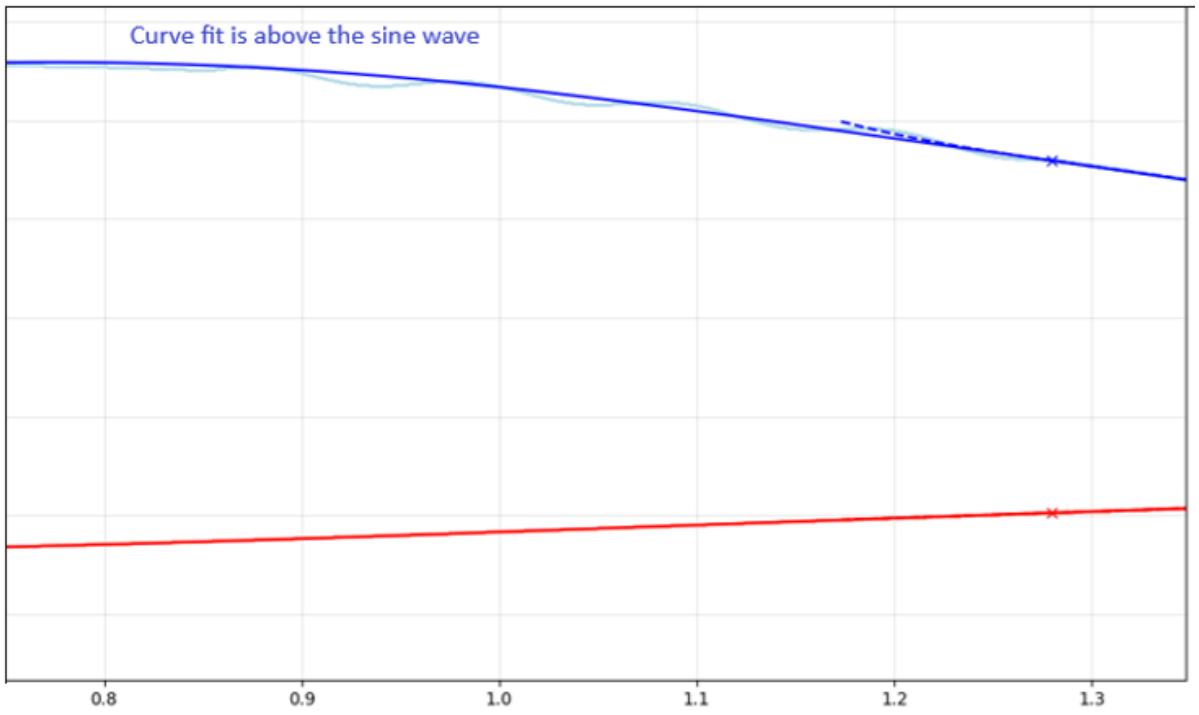


Figure 20– Quintic polynomials near the waves.

At this point we have extracted the form (the shape of the airfoil) from the 2D point cloud. When we subtract the form from the point cloud we are left with the texture. The texture consists of all the defects (such as steps, flat spots, ridges, grooves, ramps, and waves) as well as roughness (see Figure 21).

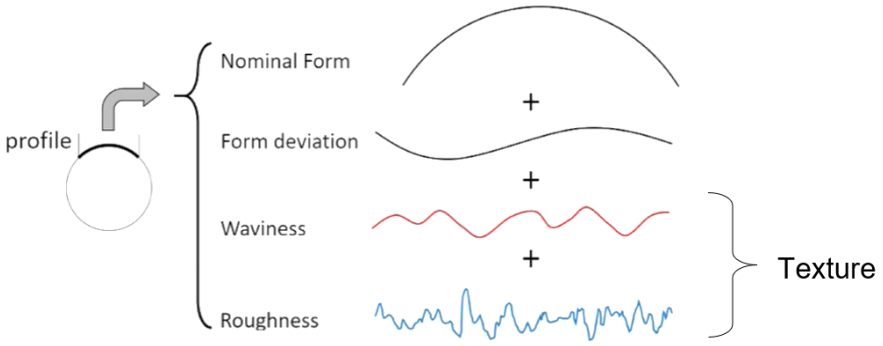


Figure 21 – Separation of form, texture, and roughness, adapted from [18].

To subtract the form from the 2D point cloud we march along the form (the line formed by the quintic polynomials) at a step size that mirrors the resolution of the point cloud, and at each point we compute the local normal. We specify a tangential tolerance and find the nearest point to the normal. The normal distance is the local texture, and we plot the texture against the surface coordinate, as shown for the top surface in Figure 22. Our attention is drawn to the spikes and to the sinusoidal waves. The spikes indicate the presence of steps, ramps, or flat spots. We note that the upstream portion of the sinusoidal waves is below the axis, as we expect by comparison to Figure 20.

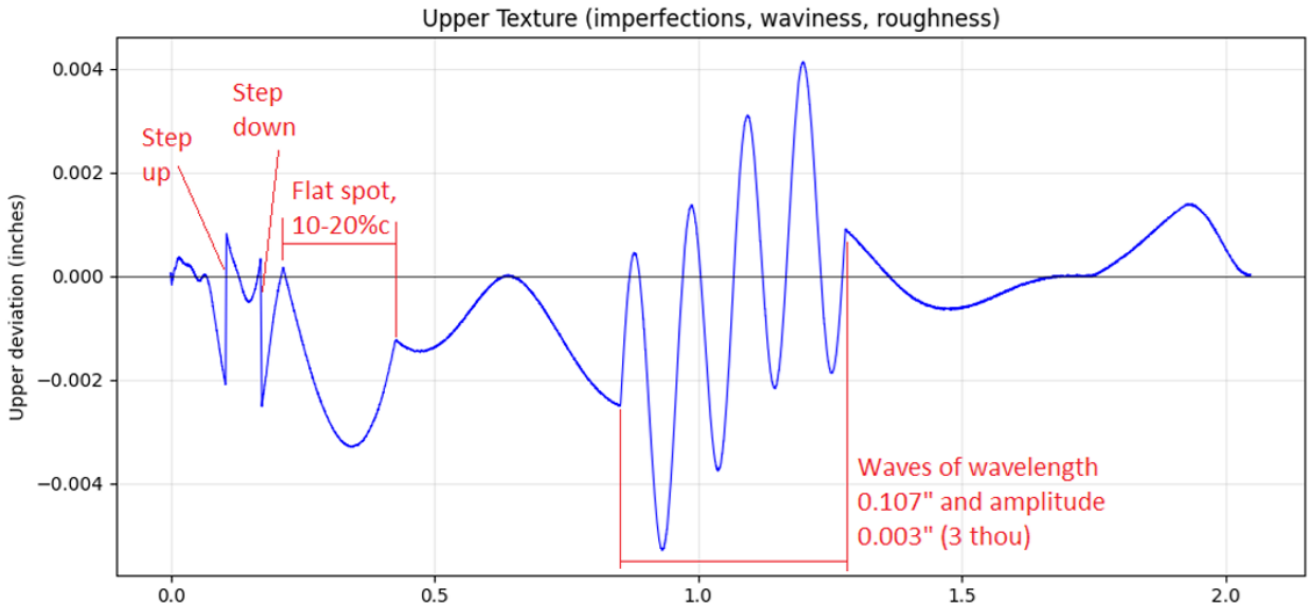


Figure 22 – Upper texture

Next, we compute and plot (Figure 23) the point-to-point slope of the texture, to more clearly mark the location with unusually high slopes.

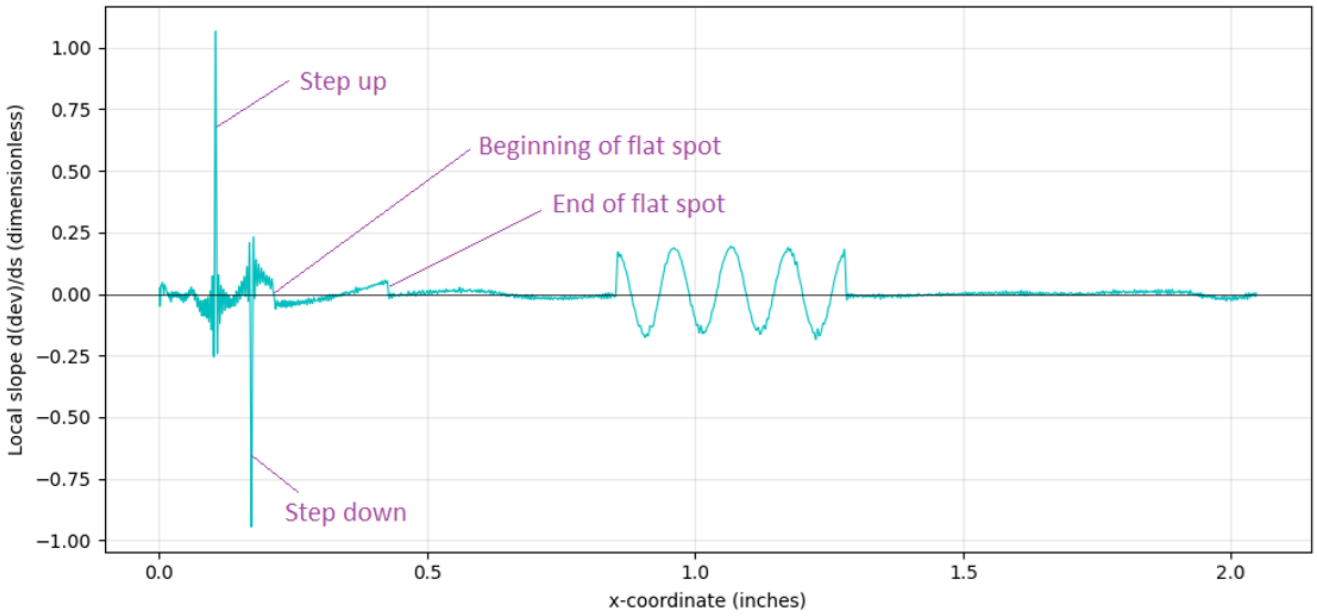


Figure 23 – Point-to-point slope of the upper texture

10. Extra Quintic Polynomials to Define Straight Lines from Steps, Ramps, Flats

It is helpful to use the locations with very pronounced slopes (at x-locations of 0.15, 0.2, 0.23, and 0.4 inches for the case shown in Figure 23) to define separate cubic and quintic polynomials that will more clearly show the local surface feature. At each x-location that features a high slope, we place a new point on the upper surface. At each point we fit two cubic polynomials which will result in two local slopes, one on either side of the point. Between any two new points that are adjacent, we then define a quintic polynomial. The purple line in Figure 24 shows the result for the flat spot.

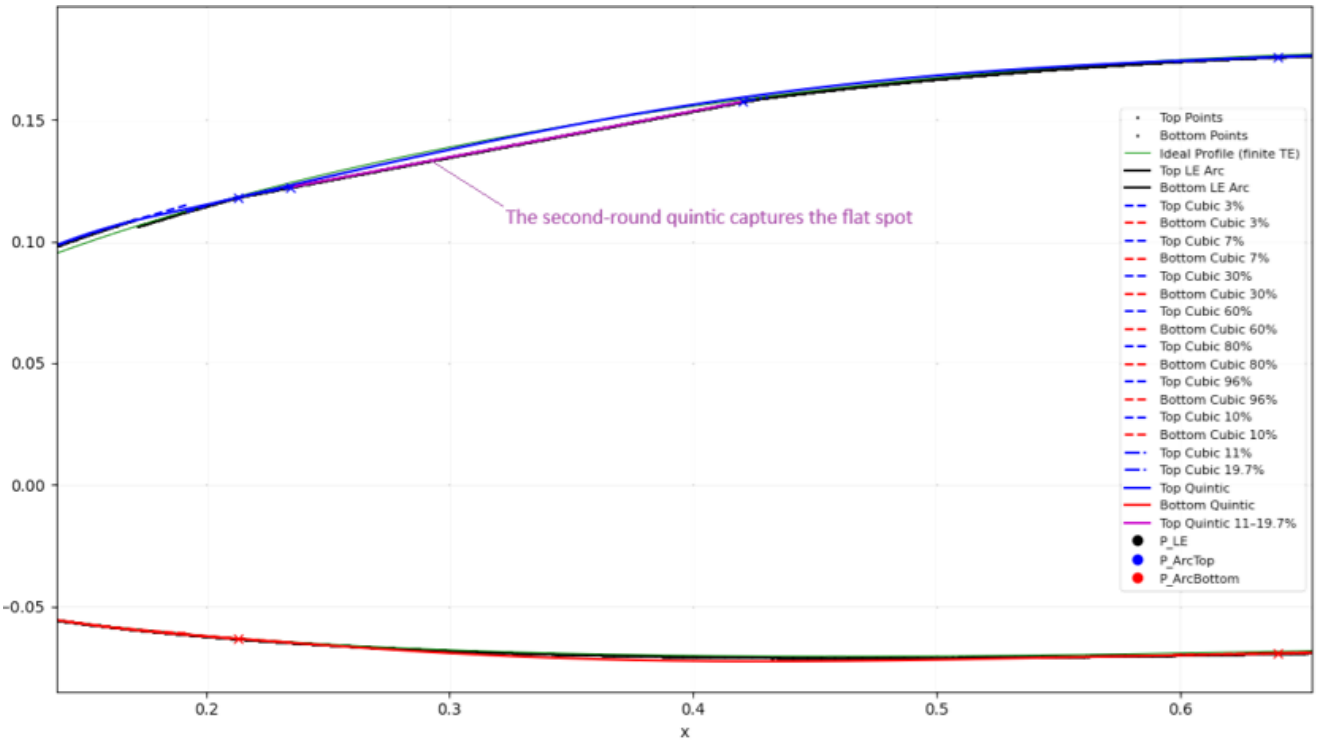


Figure 24 – Second-round quintic polynomial captures the flat spot.

11. Using FFT and Wavelet Transforms to Characterize Surface Waves

Having characterized the steps and flat spots, we move on to characterize the surface waves. We begin by refining the surface texture in Figure 22 so that it has an even spacing, and then we apply a fast Fourier Transform (FFT). The wavelength spectrum in Figure 25 shows that there is a strong sinusoidal feature that has a wavelength of about 0.1 inches, but from the figure we cannot deduce where it is, what its amplitude is, or how many periods it involves.

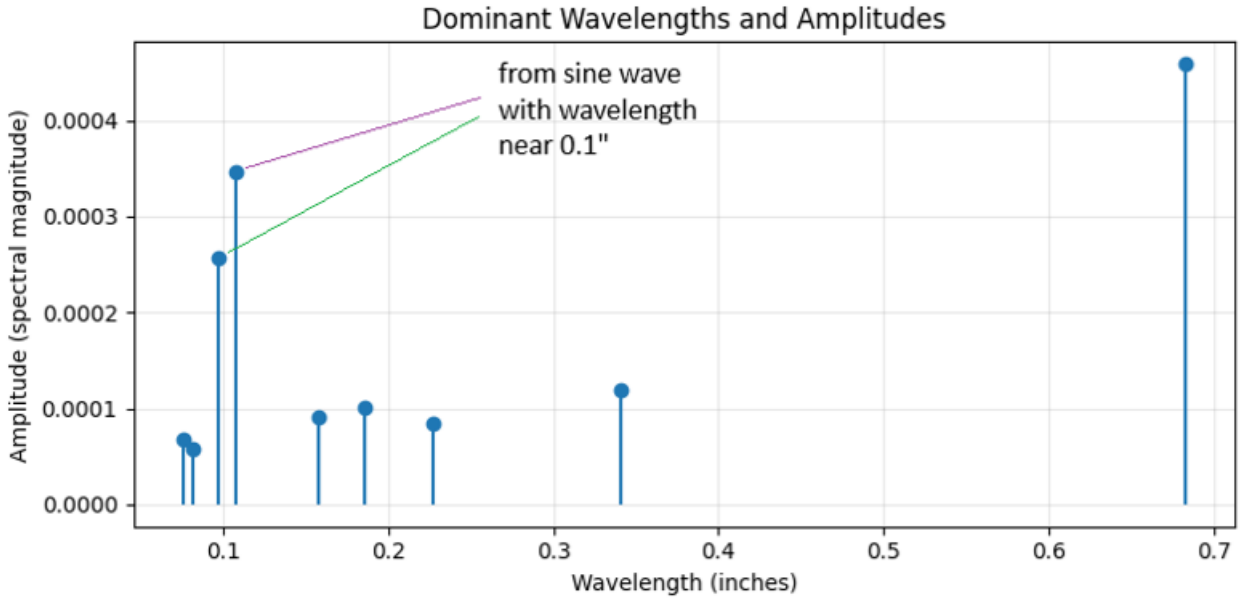


Figure 25 – Wavelength spectrum of the upper texture, from FFT.

The band contributions in Figure 26 show how the different sinusoids are superimposed to yield the overall texture (the black line). We verify that the two wavelengths near 0.1” comprise the wave train located roughly between 0.9” and 1.25”. From the FFT we might conclude that it has between four and six periods.

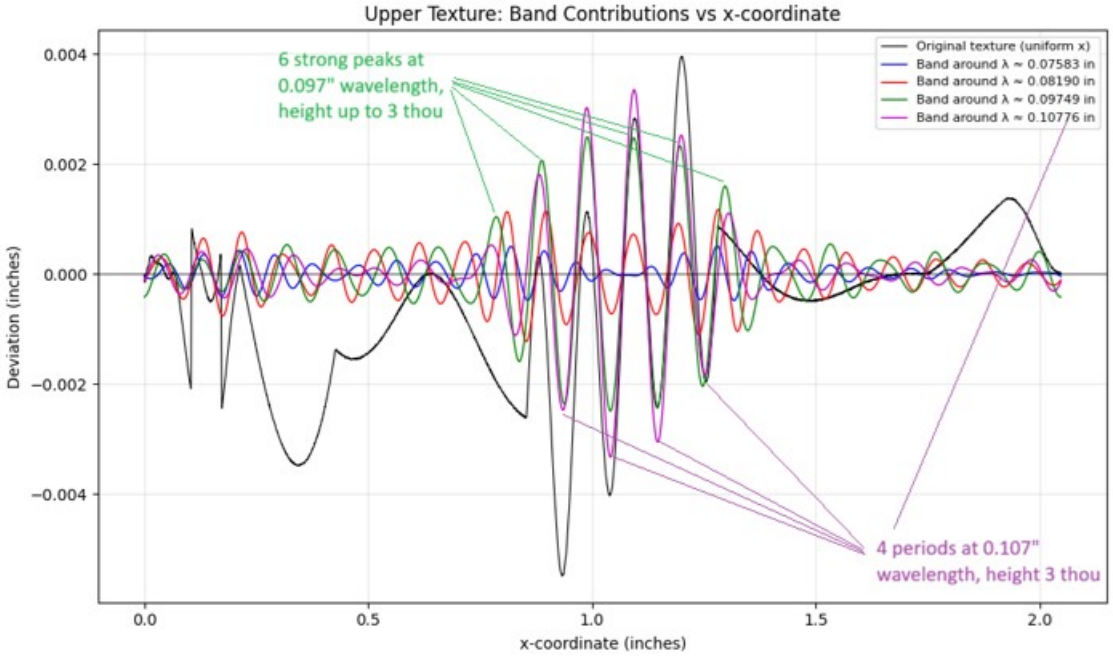


Figure 26 – Band contributions for the upper texture, from FFT.

Application of the wavelet transform provides additional insight and more clearly indicates the dominant harmonic content of the upper texture (Figure 27).

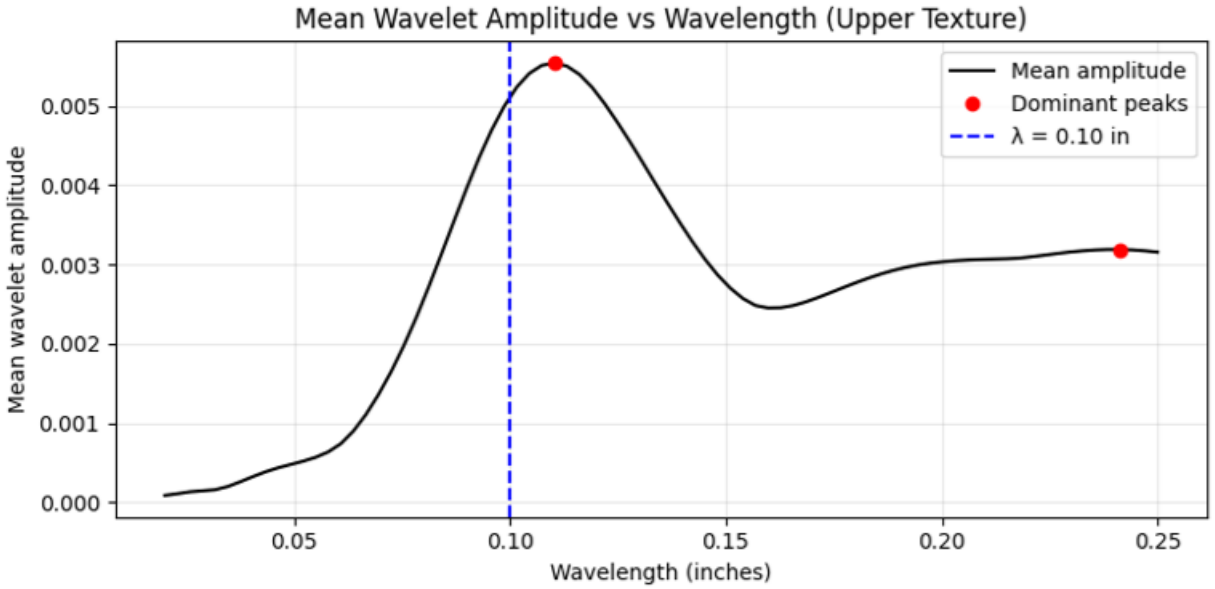


Figure 27 – Wavelet spectrum of the upper texture.

12. Application of the Process to an Airfoil with Smaller Imperfections

We created a second fake 2D point cloud (the "revised airfoil") by specifying imperfections that exactly correspond to the critical heights listed in the table shown in Figure 12. Figure 28 shows a wave of wavelength 0.25 mm (9.84 thou, or about 0.01") and trough-to-peak amplitude of 40 microns (1.57 thou) between x=0.11" and 0.32", together with a 3.54 thou (90 microns) step up at 0.135" and a step down at 0.3". Note that these imperfections are barely perceptible on a 2" airfoil.

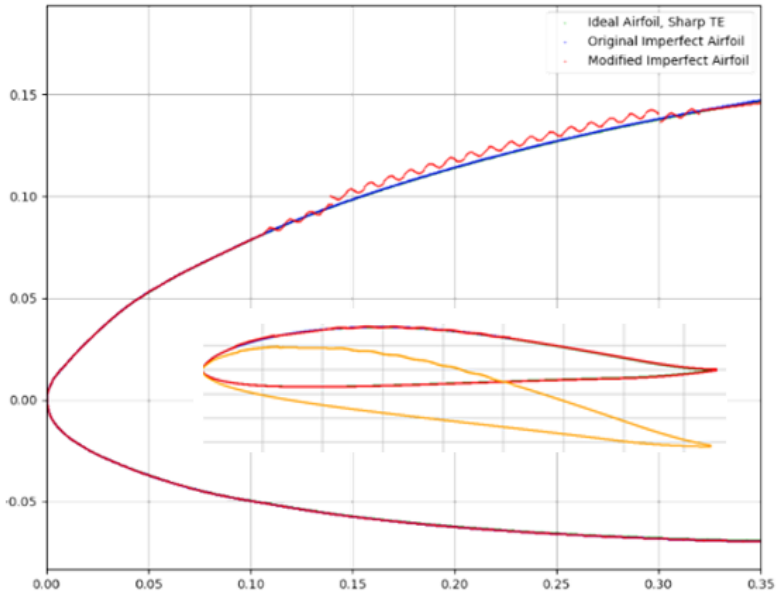


Figure 28 – Forward portion of the revised airfoil with waves and steps.

Figure 29 show that there is a flat spot between x=0.32" and 0.54". Directly after that is a dual wave train consisting of a short-wavelength (0.25 mm or 9.84 thou), low-amplitude (40 microns or 1.57 thou) wave and a longer-wavelength (3mm or 118 thou, or about 0.12") and higher amplitude (57 microns or 2.244 thou) wave that extends to x=1.3".

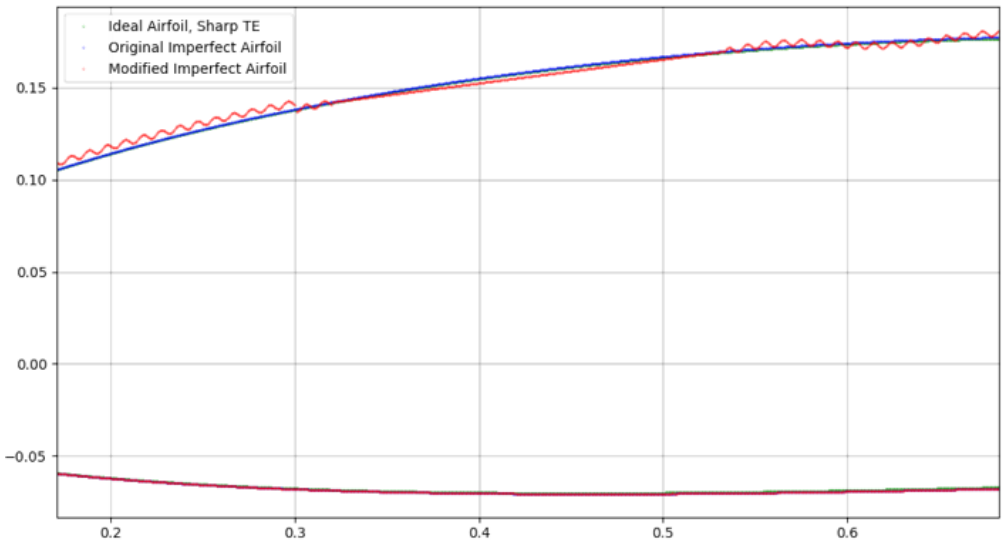


Figure 27 – Forward waves, flat spot, and mid-chord dual wave train.

The wavelength spectrum resulting from a FFT analysis of this airfoil shows (Figure 28) the two high-frequency waves with wavelength of about 0.01”, as well as the lower frequency wave with wavelength 0.12”.

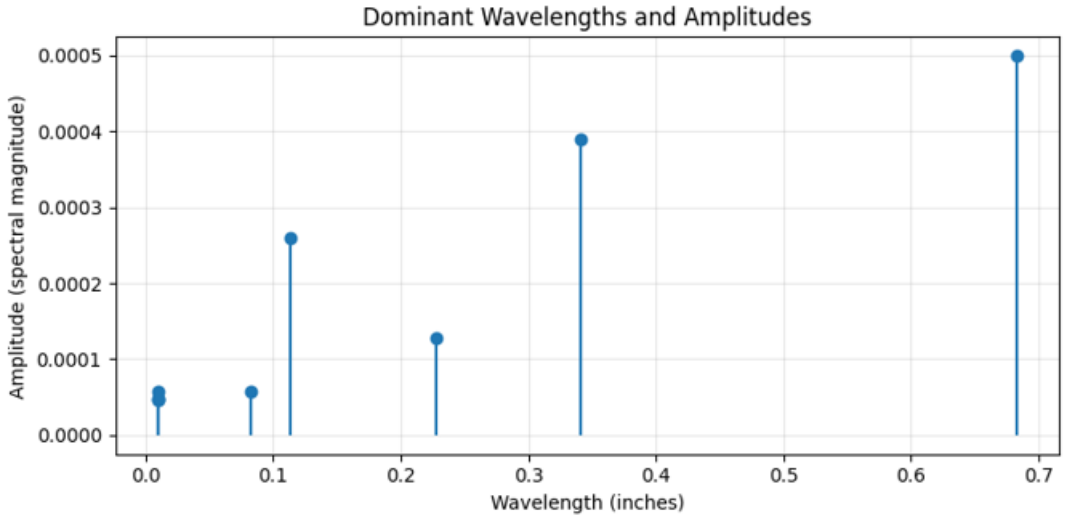


Figure 28 – FFT wavelength spectrum of the upper texture of the revised airfoil.

13. Conclusions and Future Work

In this paper we have presented a method for controlling waviness and other defects on small wind tunnel models in order to avoid undesired transition to turbulence.

We use the Van Driest and Blumer (D-B) method to find the critical heights of steps, and we use Carmichael criteria to determine the height of gaps, ramps, and waves. To determine the critical wavelengths of surface waves we use Orr-Sommerfeld stability theory for non-zero Hartree pressure parameters.

To extract the form from a given 2D point cloud we fit a partial circular arc at the LE, an isosceles trapezoid at the TE, and quintic polynomials elsewhere. We subtract the form from the point cloud to extract the texture, which we analyze using FFTs and wavelet transforms to identify dominant wavelengths.

Applying the method to a two-foot model of the PRANDTL-D flying wing we found that scanner resolutions need to be 4 microns vertically, and 11 microns horizontally.

Future work might entail verifying some of the findings in this report, to make sure that the Carmichael Criterion for wave amplitudes applies at such small Reynolds numbers. It would be useful to produce a series of rectangular wings that have the PRANDTL-D airfoil and that have different types of surface defects carefully machined into the surface. The goal would be to determine the transition location in each case, perhaps using fluorescent oil flow and/or infrared thermography (IRT). One would also scan each model and apply the methods from this paper to quantify the surface defects. The wind tunnel work would likely be carried out in a low-turbulence wind tunnel, such as the Dryden wind tunnel at USC [19].

Contact Author Email Address

Mailto: Christoph.Hiemcke@ga-asi.com

Copyright Statement

The authors confirm that they, and/or their company or organization, hold copyright on all of the original material included in this paper. The authors also confirm that they have obtained permission, from the copyright holder of any third party material included in this paper, to publish it as part of their paper. The authors confirm that they give permission, or have obtained permission from the copyright holder of this paper, for the publication and distribution of this paper as part of the ICAS proceedings or as individual off-prints from the proceedings.

References

[1] Siim Sild. Profile of a Surface (GD&T) Explained. 2022. https://fractory.com/profile-of-a-surface-gdt-explained/. Accessed 1 Oct 2025.

[2] Hamid Ghorbani and Farbod Khameneifar (Polytechnique Montreal). Airfoil profile reconstruction from unorganized noisy point cloud data. *Journal of Computational Design and Engineering*, Volume 8, Issue 2, April 2021, Pages 740–755.

[3] How to perform a profile form & position inspection in ZEISS INSPECT Airfoil (4/7). https://www.youtube.com/watch?v=nj1eLjpayHI. Accessed 1 Oct 2025

[4] Airfoil Inspection - the app for blade geometries. Nov 2024. https://www.youtube.com/watch?v=p6DeaWGeYL4. Accessed 1 Oct 2025.

[5] Jonas Aust, Dirk Pons (University of Canterbury NZ). Comparative Analysis of Human Operators and Advanced Technologies in the Visual Inspection of Aero Engine Blades. *MDPI Applied Sciences* 12(4): 2250. February 2022.

[6] Yanyan Guo, Wantao HeKai Zhong, Chungang Zhuang, Tao Chen, Hongjun Zhang. Automatic and high-accuracy matching method for a blade inspection system integrating fringe projection profilometry and conoscopic holography. *IOP: Meas. Sci. Technol*. 34 (2023): 075011 (11 pp).

[7] Ellande Tang, Soon-Jo Chung (CalTech). Rapid extraction of propeller geometry using photogrammetry. *International Journal of Micro Air Vehicles* 14, 1-22. October 2022.

[8] Yuichiro Tobita (SDSU), Patrick Hammer (AFRL), Christoph Hiemcke, Xiaofeng Liu (SDSU). Prandtl-D Flying-Wing Wind Tunnel Aerodynamic Characterization and Surface Flow Survey. *AIAA SciTech 2026*. AIAA-2026-1892.

[9] D. Philpott. Use of local-flow conditions for calculation of roughness-particle height in transition strips on wings. Associated software: ecrit2. *ESDU 09016*, Feb 2013.

[10] Clifford J. Obara, Bruce J. Holmes (NASA Langley). Roughness and Waviness Requirements for Laminar Flow Surfaces. *NASA Langley Symposium on Aerodynamics*, Volume 1, 1986. Pages 519-537.

[11] Bruce H. Carmichael. Prediction of Critical Reynolds Number for Single Three Dimensional Roughness Elements. *NAI-58-412 (BLC-109)*, Northrop Aircraft, Inc., Beverly Hills, CA, May 1958.

[12] China Jiakuan Xu, Junqiang Bai, Lei Qiao, Yang Zhang, Ziyuan Fu (Northwestern Polytechnical University, China). A Linear Stability Theory-Based Transition Model Using Local Variables for RANS Simulations of Transitional Flow. AIAA-2016-3490.

[13] Texture International Standards Organization (ISO). Geometrical Product Specifications (GPS) — Indication of surface texture in technical product documentation. ISO 1302:2002(E). Superseded by ISO 21920-1:2021. https://cdn.standards.iteh.ai/samples/28089/bbc16b31517b4ce1b405039b3906eee8/ISO-1302-2002.pdf. Preview accessed 17 Oct 2025.

[14] Keyence Corporation. Introduction to Roughness. Accessed 17 Oct 2025. https://www.keyence.com/ss/products/microscope/roughness/line/roughness-symbols.jsp.

[15] Marco (last name not given in the posting). OpenVSP 3 model of the H IV. https://groups.google.com/g/openvsp/c/n8nciixz5-o. Accessed 25 September 2024.

[16] Albion H. Bowers, Oscar J. Murillo (NASA Armstrong/Edwards), Robert "Red" Jensen, Brian Eslinger (Jacobs), Christian Gelzer (Logical Innovations). *On Wings of the Minimum Induced Drag: Spanload Implications for Aircraft and Birds*. NASA/TP – 2016-219072.

[17] Christoph Hiemcke. Translation of Airfoil Designer's Geometric Parameters into Quintic Polynomials for Optimizing Thickness and Camber, with Historical Notes. *AIAA AVIATION 2025, Las Vegas*. AIAA-2025-3446.

[18] Francois Blateyron (Digital Surf). Surface Metrology Guide: Introduction to filtration in surface metrology. 9 August 2023. Accessed 20 Oct 2025. 20 minutes. https://www.youtube.com/watch?v=2OMrfNUt0T4.

[19] Spedding, Geoffrey R. History (of the Dryden Wind Tunnel at USC). Website, 5/24/2023, accessed 9 April 2026. https://sites.usc.edu/drydenwt/history/.